

# Two-way single-photon-level photonic conversion between 852nm and 1560nm for connecting cesium D2 transition with telecom C-band

Kong ZHANG<sup>1</sup>, Jun HE<sup>1,2</sup>, and Junmin WANG<sup>1,2,\*</sup>

<sup>1</sup>*State Key Laboratory of Quantum Optics and Quantum Optics Devices, and Institute of Opto-Electronics, Shanxi University, Tai Yuan 030006, People's Republic of China*

<sup>2</sup>*Collaborative Innovation Center of Extreme Optics of the Education Ministry and Shanxi Province, Shanxi University, Tai Yuan 030006, People's Republic of China*

A compact setup for two-way single-photon-level photonic conversion between 852 nm and 1560 nm has been implemented with the same periodically-poled magnesium-oxide-doped lithium niobate (PPMgO:LN) bulk crystals for connecting cesium atomic D2 transition (852 nm) to telecom C-band. By single-pass mixing a strong continuous-wave pump laser at 1878 nm and the single-photon-level periodical signal pulses with a mean photon number of  $\sim 1$  per pulse in a 50-mm-long PPMgO:LN bulk crystal, the conversion efficiency of  $\sim 1.7\%$  ( $\sim 2.0\%$ ) for 852-nm to 1560-nm down-conversion (1560-nm to 852-nm up-conversion) have been achieved. We analyzed noise photons induced by the strong pump laser beam, including the spontaneous Raman scattering (SRS) and the spontaneous parametric down-conversion (SPDC) photons, and the photons generated in the cascaded nonlinear processes. The signal-to-noise ratio (SNR) has been improved remarkably by using the narrow-band filters and changing polarization of the noise photons in DFG process. With further improvement of the conversion efficiency by employing PPMgO:LN waveguide, instead of bulk crystal, our study may provide the basics for cyclic photon conversion in quantum network.

## I. INTRODUCTION

The idea of constructing quantum internet was proposed in 2008 [1]. Implementation of long-distance quantum information network requires the quantum nodes which store and process quantum information and the low-loss optical fiber networks which connect the nodes by flying photonic qubits. The photonic frequency of quantum nodes are usually much higher than that of flying photonic qubits transmitted in the low-loss optical fiber networks. Therefore, it needs quantum frequency conversion (QFC) [2, 3] of the photonic frequency between the quantum nodes and the flying photonic qubits. Several qubit platforms, such as trapped ions [4], trapped cold single atom or cold atomic ensemble [5, 6], quantum dots [7], and etc have been demonstrated for building quantum nodes for the quantum network. In 2012, two groups firstly demonstrated QFC [8, 9]. Zaske *et al* [8] demonstrated efficient ( $\sim 30\%$ ) quantum frequency conversion of visible single photons (711 nm) emitted by a quantum dot (QD) to a telecom wavelength (1313 nm) and the signal-to-noise ratio (SNR) was  $\sim 50$ . Ates *et al* [9] combined single photons from an InAs/GaAs QD at 980 nm with a 1550-nm pump laser in a periodically poled lithium niobate (PPLN) waveguide to generate 600-nm photons with the internal conversion efficiency of 70% and SNR of 100. In 2014, Albrecht *et al* [10] demonstrated converting 780-nm single photons into 1552-nm telecom C-band with a maximum conversion efficiency of  $\sim 13.6\%$  based on PPLN waveguide and the maximum SNR of 85. In 2018, Dreau *et al* [11] converted spin-selective photons at 637 nm, associated with the coherent nitrogen-vacancy zero-phonon line, to the target

wavelength of 1588 nm, the conversion efficiency was  $\sim 17\%$  and the SNR was  $\sim 7$ . Many groups have also reported relevant research works [12-17].

Most of the above-mentioned conversions aimed at red spectral ranges converted to telecom bands. However, inverse conversions are also important. In 2011, Huang *et al* [18] detected photons at  $1.04\ \mu\text{m}$  via coincidence frequency upconversion to  $0.62\ \mu\text{m}$ . A total detection efficiency of  $\sim 3.7\%$  was achieved with a quite low noise probability per pulse of 0.0002. In 2018, Ma *et al* [19] used 1550 nm and 1950 nm two wavelengths pump each other to yield 864 nm by using PPLN waveguide with a conversion efficiencies of  $\sim 28\%$  and  $\sim 27\%$  respectively. In 2018, Wright *et al* [20] reported two-way photonic interface for linking 422 nm to the telecom C-band, and achieved up-conversion (down-conversion) at single-photon level with conversion efficiency of  $\sim 9.4\%$  ( $\sim 1.1\%$ ), and SNR of  $\sim 39.4$  ( $\sim 108$ ). The up-conversion single-photon detector (SPD) using this scheme can extend the well-developed silicon based single-photon detector to telecom C-band.

Now we consider a simple quantum network shown in Fig. 1 for single-photon distributing and storing. The left node is single-cesium (Cs)-atom optical tweezer based 852-nm single-photon source [21-23], while the right node is cold or hot Cs atomic ensemble. These two nodes can be connected by ultralow loss 1560-nm telecom single-mode fiber. By employing QFC1, the 852-nm single photons emitted by the left node can be converted to 1560-nm single photons, which served as the flying photonic qubits for single-photon distributing via long-distance 1560-nm telecom fiber link. Then by employing QFC2, 1560-nm single photons can be converted back to 852-nm single photons, which can interact with the right node via Raman-type memory or the electro-magnetically induced transparency (EIT) - type memory protocols for single-

\* Corresponding Author: wwjjmm@sxu.edu.cn

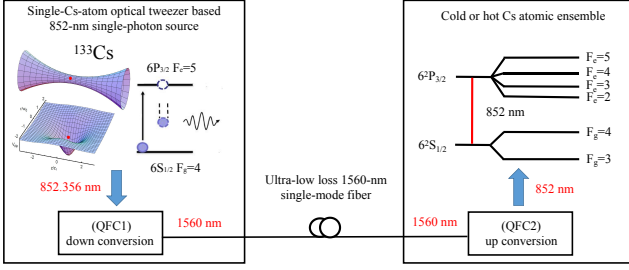


FIG. 1. Schematic diagram of two-way QFC for distributing and storing single photons. The left node is single-cesium (Cs)-atom optical tweezer based 852-nm single-photon source, while the right node is cold or hot Cs atomic ensemble. These two nodes can be connected by low-loss 1560-nm telecom single-mode fiber. By employing QFC1 the 852-nm single photons emitted by the left node can be converted to 1560-nm single photons served as the flying photonic qubits, and then can be converted by employing QFC2 back to 852-nm single photons which interact with the right node.

photon storing. We have experimentally achieved 852-nm single-photon source based on single-Cs-atom optical tweezer [21-23], and we plan to build QFC1 and QFC2 converters for implementation of single-photon distributing and storing protocols.

In this paper, we demonstrated two-way down-conversion and up-conversion between 852 nm and 1560 nm based on single-pass PPMgO:LN bulk crystal for connecting 852-nm Cs D2 transition and 1560-nm telecom C-band at single-photon level (one photons per pulse). The efficiency is mainly limited by spatial mismatch in the bulk crystal, and it is hard to effectively use bulk crystal because the beams are focused. These problems can be avoided by using a waveguide, and the efficiency will be improved. So we pay more attention to improving SNR. First, we analyzed the noise photons induced by a strong pump laser beam in PPMgO:LN crystal, such as the spontaneous Raman scattering (SRS) and the spontaneous parametric down-conversion (SPDC) photons, as well as the photons generated in the cascaded nonlinear processes. Then, we enhance SNR by using the narrow band-pass filters. Moreover, by rotating the polarization of the output photons, the noise photons are filtered by PBS at the expense of extraction efficiency in DFG experiment.

## II. DFG FROM 852-NM TO 1560-NM PHOTONS: EXPERIMENT AND RESULTS

In this part, we convert 852 nm photons to 1560 nm photons by DFG and enhance the SNR by using the narrow band-pass filters and changing the polarization of the noises. At the same time, we also analyze the noise photons induced by the strong pump beam. Fig. 2 (a) is diagram of single-photon-level DFG conversion. The experimental setup is shown in Fig. 2 (b). A master-

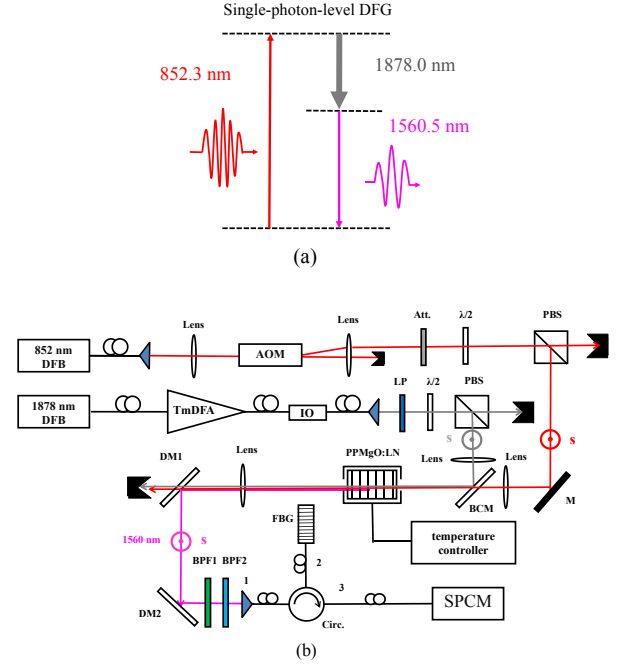


FIG. 2. (a) Diagram of single-photon-level DFG photonic conversion. (b) The experimental setup for DFG. The s-polarization 852-nm photons are converted to 1560-nm photons with PPMgO:LN crystal by DFG pumped by the s-polarization 1878-nm strong laser beam. DFB: distributed feedback diode laser; TmDFA: Thulium-doped fiber amplifier; OI: optical isolator; AOM: acoustic optical modulator;  $\lambda/2$ : half-wave plate; PBS: polarization beam splitter cube; Att.: attenuator; s: s polarization; BCM: beam-combination mirror; DMs: 1560-nm high-reflection, 852-nm and 1878-nm high-transmission dichromatic mirrors; BPFs: narrow 1560-nm band-pass filters; Circ.: fiber circulator; FBG: fiber Bragg grating filter ( $\sim 0.3$  nm); SPCM: single-photon counting module.

oscillator power amplifier (MOPA) consists of a compact distributed feedback (DFB) diode laser and a Thulium-doped fiber amplifier (TmDFA) can provide watt-level single-frequency narrow-band 1878-nm pump light. As we know, the wavelength of commercial TmDFA is 1920 nm - 2200 nm, while the 1878-nm TmDFA used in experiment is produced with special technique. An optical isolator is used to restrain the laser feedback, thus ensuring the stability of TmDFA. To simulate single-photon pulses, a compact DFB diode laser at 852 nm, an acoustic-optical modulator (AOM) and a strong attenuator are employed to chop and weaken 852-nm continuous-wave laser beam to 1-MHz repetition rate and 500-ns duration square-wave periodical optical pulses with a mean photon number per pulse is  $\sim 1$ . Then, a 50-mm-long PPMgO:LN bulk crystal (the thickness: 0.5 mm; the poling period:  $23.4 \mu\text{m}$ ; Type-0 quasi-phase matching; The both flat ends of the crystal were anti-reflection coated for 852 nm, 1560 nm, and 1878 nm, and the residual reflectivity  $R < 0.2\%$ ) fabricated by HC Photonics is employed for single-photon level photonic conversion. The crystal is

placed in a home-made oven, which is made of red copper and precisely temperature stabilized by using a temperature controller (Newport Corp., Model 350B). We can achieve the optimized phase matching by adjusting the temperature of the crystal.

For laser frequency conversion with a bulk nonlinear crystal, the beam waist of the focused laser beam in the crystal should match the crystal length [24], and the optimum B-K focus factor  $\xi = 2.84$  [25] is a non-negligible parameter. We choose two lenses ( $f = 75$  mm) to focus 1878-nm and 852-nm laser beams separately, then combine two beams via a dichromatic mirror (BCM) to avoid the chromatic aberration in the case of using one focusing lens for these two beams. After the crystal, a lens ( $f = 75$  mm) is used to collimate the output beams. The 1560-nm telecom photons were separated with residual signal photons at 852 nm and pump laser beams at 1878 nm by using two dichromatic mirrors (DMs), and then passed through the 1560-nm band-pass filters (BPFs) (the 50-nm HMFV bandwidth BPF:  $T = 92\% @ 1560$  nm,  $T \sim 1E-4 @ 852$  nm (OD4) and  $T \sim 30\% @ 1878$  nm; the 12-nm HMFV bandwidth BPF:  $T = 74\% @ 1560$  nm,  $T \sim 1E-5 @ 852$  nm (OD5) and  $T \sim 1E-4 @ 1878$  nm (OD4)) and a fiber Bragg grating (FBG) filter (center wavelength  $\sim 1560.59$  nm, HMFV bandwidth  $\sim 0.3$  nm,  $R = 92\% @ 1560$  nm) to improve the SNR. Finally, the 1560-nm telecom photons are counted by a single-photon counting module (SPCM) (Aurea; quantum efficiency  $\sim 15\%$  and dark count rate  $\sim 1700$  counts/s).

First, we find the optimized phase matching condition by adjusting the PPMgO:LN crystal's temperature in single-pass DFG experiment. When the optical power of the 1878-nm pump beam was  $\sim 450$  mW, the phase matching is achieved at a temperature of  $\sim 78.9$  °C, as shown in Fig. 3.

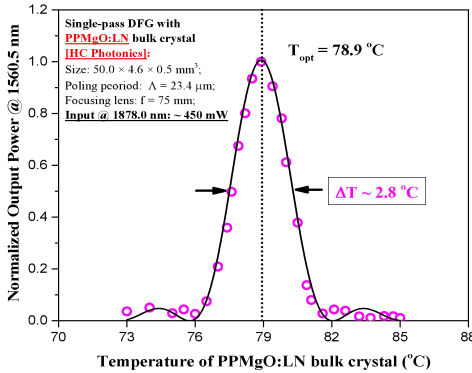


FIG. 3. Temperature dependence of 1560.5-nm output power in the case of DFG. The open circles represent the experimental data, while the solid line is theoretical fitting curve. The optimal quasi-phase-matching temperature is  $\sim 78.9$  °C, and the temperature bandwidth is  $\sim 2.8$  °C.

Then, we pay more attentions to the noise photons induced by the strong pump beam. In the experiment of single-photon-level photonic conversion, pump laser with

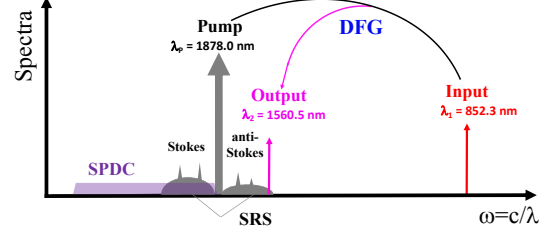


FIG. 4. Overview of DFG photonic conversion process from 852.3 nm to 1560.5 nm with the 1878.0-nm pump laser and the strong pump induced nonlinear processes. SPDC: the spontaneous parametric down-conversion (marked by the cyan grid part); SRS: the spontaneous Raman scattering (Stokes photons and anti-Stokes photons and marked by the dark grey part). The narrow BPFs and the ultra-narrow FBG can be utilized to remove the noise photons located at the target output.

long wavelength can minimize the influence of noises [15, 16]. Therefore, we chose 1878 nm laser as pump laser from the scheme of 551 nm and 1878 nm lasers. Fig. 4 shows the overview of DFG photonic conversion process from  $\lambda_1 = 852.3$  nm to  $\lambda_2 = 1560.5$  nm with the  $\lambda_p = 1878.0$  nm pump laser and the strong pump induced nonlinear processes (SPDC and SRS). First, the wavelength of SPDC photons (marked by the cyan gridding part) are longer than the pump laser, it is far away from the targeted photons, so we assume that SPDC photons of the pump light can be excluded in our case. Then SRS photons (marked by the dark grey part) distribute on both sides of the pump light, and the target photons are located in the weak anti-Stokes region, so the main noise source in this process are anti-Stokes photons. The narrow BPFs and the ultra-narrow FBG can be utilized to remove the noise photons located at the target output. In addition, the TmDFA in experiment is not commercial, so it may generate more noises, which will reduce the SNR.

In the experiment, the conversion efficiency is defined as  $\eta = N_{out}/N_{in}$ , we define  $N_{in}$  as the count rate of signal photons in the front of the crystal, and  $N_{out}$  as the count rate of target photons at the end of the crystal. The influence of noise photons at target wavelength induced by the strong pump light is inevitable. Therefore, we define  $N_{out} = N_{p+s} - N_p$ , where  $N_{p+s}$  is the count rate of the detector at 1560 nm when both pump and signal photons are coupled into the crystal, and  $N_p$  is the count rate of the detector at 1560 nm when only pump light is present in the crystal (signal photons blocked). Zaskie *et al* [15] defined the conversion efficiency in this way. Fig. 5 shows the DFG conversion efficiency and SNR with different filters versus pump power. The SNR can slightly improve by using narrower filters. Fig. 5 (a) is the result for a BPF with  $\sim 50$ -nm HMFV bandwidth (transmittance:  $92\% @ 1560$  nm and optical density (OD) 4), and the SNR is 19.5. Then the SNR can be improved to 31.3 by using a BP filter with  $\sim 12$ -nm HMFV bandwidth (transmitt-

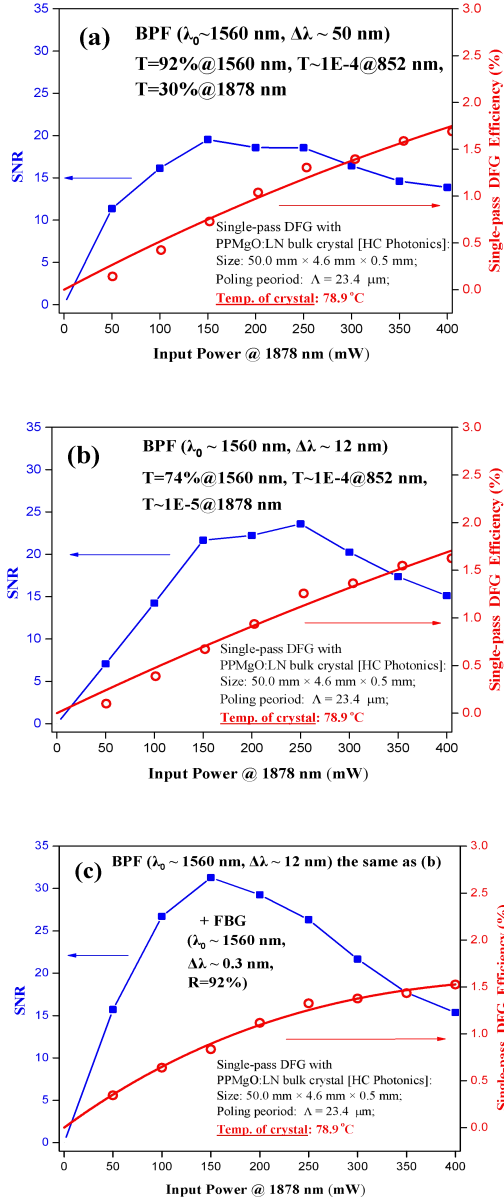


FIG. 5. DFG conversion efficiency and SNR with different filters versus the 1878-nm pump power. The squares represent the SNR, and the circles represent the DFG conversion efficiency. (a) The results for a BPF with  $\sim 50$ -nm HMFV bandwidth; (b) The results for a BPF with  $\sim 12$  nm HMFV bandwidth; (c) The results for combination of a BPF with  $\sim 12$ -nm HMFV bandwidth and a ultra-narrow-band FBG filter with  $\sim 0.3$ -nm HMFV bandwidth.

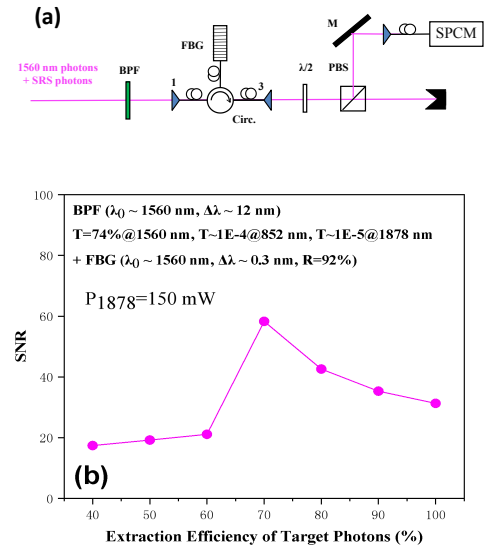
ance: 74%@1560 nm and OD4) combined a FBG filter with  $\sim 0.3$ -nm HMFV bandwidth (reflectivity: 92% @1560 nm and OD1, SM) in Fig. 5 (c). Noise photons reduce from 372 counts/s to 266 counts/s. Therefore, the SNR will be increased by using narrower bandwidth of the filters theoretically. However, when using a very narrow filter (the bandwidth is much smaller than the filter used in our experiment), the SNR is not significantly improved. In the result of conversion efficiency, the solid

lines represent the fitting to Eq. (1):

$$\eta(P_p) = \eta_{max} \sin^2(L\sqrt{\eta_n P_p}) \quad (1)$$

Where  $L$  is the length of the non-linear medium,  $P_p$  is the injected pump power, and  $\eta_n$  is a conversion parameter characteristic to the specific device. However, the curvature of curve (a) and (b) are different from (c), which may be due to the bandwidth of filters, and the efficiency in Fig. 5 (c) is close to saturation, which is mainly caused by the photons consumption ratio of signal photons to pump photons. The maximum DFG internal conversion efficiency is 1.7% when signal level is set to  $10^6$  photons  $s^{-1}$  with a mean photon number per pulse is  $\sim 1$ . The efficiency is main limited by spatial mismatch in PPLN crystal [26], and we cannot use crystal completely because the beams are focused. These two problems can be effectively avoided by using a waveguide, and the efficiency will be improved. Last, the inverse SFG (from 1560 nm to 852 nm photons) will be occurred under the similar condition. Therefore, we think it is inevitable that the SFG experiment will be happen in the DFG experiment. This means that the 1560 nm photons generated by the DFG may be further converted back to 852 nm photons in the crystal. Although the conversion efficiency is proportional to the power of the input laser in the single-pass configuration [27-29], the inverse conversion efficiency is lesser than the target conversion efficiency, that factor may also limits our DFG efficiency.

Although the PPMgO:LN crystal we used is type-0 quasi-phase matching (852-nm, 1878-nm and 1560-nm photons are all with s polarization), the noise photons (mainly are anti-Stokes photons of SRS induced by the strong 1878-nm pump laser beam) may be elliptically polarized with a special preponderant direction due to inhomogeneity of the crystal. Based on this point, we try to improve SNR by changing the polarization of output





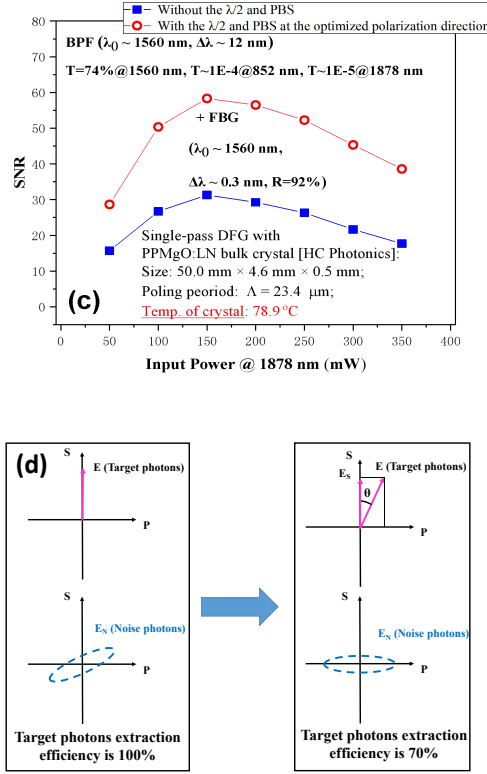


FIG. 6. The results of improving SNR by changing polarization of output photons. (a) The experimental setup for polarization optimization. BPF: a 1560-nm band-pass filter with  $\sim 12$ -nm HMF bandwidth ( $T = 74\%$ @1560 nm,  $T \sim 1E-4$ @852 nm,  $T \sim 1E-5$ @1878 nm); Circ.: single-mode fiber circulator; FBG: 1560-nm fiber Bragg grating filter with 0.3-nm HMF bandwidth ( $R = 92\%$ @1560 nm);  $\lambda/2$ : half-wave plate; PBS: polarization beam splitter cube; SPCM: single-photon counting module. (b) SNR versus target photons extraction efficiency. When the pump laser is 150 mW, the SNR can be improved to 58.3 with  $\sim 70\%$  extraction efficiency. (c) SNR versus 1878-nm pump power. The squares represent SNR without the  $\lambda/2$  plate and PBS, and the circles represent SNR with the  $\lambda/2$  plate and PBS at the optimized polarization direction (extraction efficiency is  $\sim 70\%$ ). The best SNR increases from 31.3 to 58.3. (d) The polarization of target photons and noise photons versus different extraction efficiency.  $E$  is linear polarization for the target photons and  $E_N$  is elliptical polarization for noise photons (anti-Stokes photons). The left side shows the polarization of target photons and noise photons when the extraction efficiency is 100%, and the right side shows the polarization when the extraction efficiency is  $\sim 70\%$  (after polarization rotation with an angle  $\theta \sim 33^{\circ}$ ).

photons by using of the setup shown in Fig. 6 (a). The output target 1560-nm photons and some anti-Stokes photons together pass through all the DMs and BPF as well as FBG filter, then we change their polarization by  $\lambda/2$  plate and count the reflection photons of PBS. The Circ and FBG filter are both single-mode modules, and are not sensitive to polarization. Fig. 6 (b) shows SNR versus target 1560-nm photons extraction efficiency. By

rotating  $\lambda/2$  plate, the photon counts of reflection channel are reduced, and the preponderant direction of noise photons are changing to p. SNR can be improved to 58.3 with  $\sim 70\%$  extraction efficiency. We can derive the polarization rotation angle according to different extraction efficiency by Malus law. When the extraction efficiency is  $\sim 70\%$ , the polarization rotation angle is  $\sim 33^{\circ}$ .

Fig. 6 (c) shows the results for SNR versus 1878-nm pump power. The squares represent SNR without the  $\lambda/2$  plate and PBS, and the circles represent SNR with the  $\lambda/2$  plate and PBS at the optimized polarization direction (extraction efficiency  $\sim 70\%$ ). The best SNR increases from 31.3 to 58.3. Fig. 6 (d) shows polarization of target photons and anti-Stokes photons before and after polarization optimization. The left side shows the polarization of target photons and noise photons when the target photons' extraction efficiency is  $\sim 100\%$ , while the right side shows the polarization when the target photons' extraction efficiency is  $\sim 70\%$ . The polarization rotation angle  $\theta \sim 33^{\circ}$ . The picture in Fig. 6(d) can correctly describe the measured data in Fig. 6(b).

### III. SFG FROM 1560-NM TO 852-NM PHOTONS: EXPERIMENT AND RESULTS

In this part, we convert 1560 nm photons to 852 nm photons by SFG and analyze the noise photons induced by the strong 1878-nm pump laser beam. Fig. 7 (a) is diagram of single-photon-level SFG photonic conversion. The experimental setup for SFG is shown in Fig. 7 (b). To simulate single-photon pulses, a compact DFB diode laser at 1560 nm, an AOM, and a strong attenuator are employed to chop and weaken 1560-nm continuous-wave laser beam to 1-MHz repetition rate and 500-ns duration square-wave periodical optical pulses with a mean photon number per pulse is  $\sim 1$ . The strong field is same as difference-frequency experiment. Then, the same 50-mm-long PPMgO:LN crystal is used as SFG crystal. We choose two  $f = 75$  mm lenses to focus 1878-nm and 1560-nm laser beams separately, then combine two focused beams in the PPMgO:LN bulk crystal, to avoid the chromatic aberration in the case of using one focusing lens for these two wavelengths. After crystal, a 75-mm lens is used to collimate the output laser, and output lasers spectrally separated by high-pass filters (HPFs) (852-nm high-transmission, 1560-nm and 1878-nm high-reflection mirrors). Then the 852 nm photons passed through the 852-nm band-pass filter (BPF) (transmittances:  $\sim 75\%$ @852 nm,  $\sim 44\%$ @1560 nm and  $\sim 35\%$ @1878 nm, HMF bandwidth: 0.5 nm, OD4). Finally, the 852 nm photons are counted by a SPCM (PerkinElmer Optoelectronics; SPCM-AQR-15; quantum efficiency  $\sim 48\%$  and dark count rate  $< 50$  counts/s).

In the single-pass SFG experiment, we find the optimized phase matching by adjusting the temperature of the PPMgO:LN crystal. When the power of the 1878-nm fundamental wave is  $\sim 450$  mW, the best phase matching

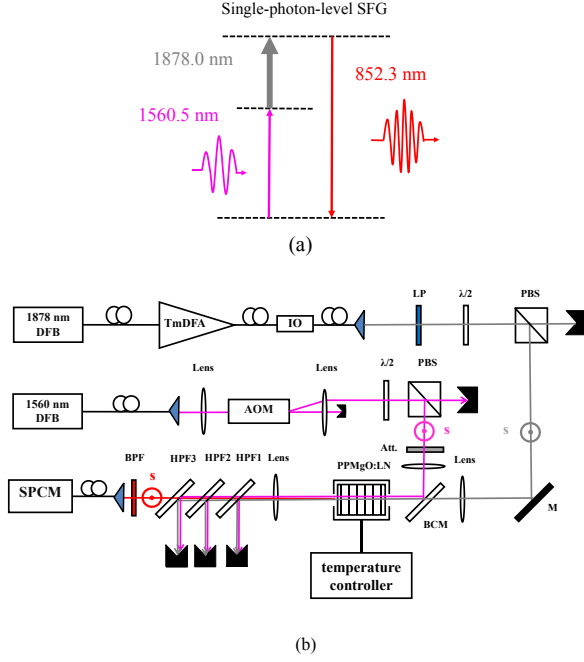


FIG. 7. (a) Diagram of single-photon-level SFG photonic conversion. (b) The experimental setup for DFG, the s-polarization 1560-nm photons are converted to 852-nm photons with PPMgO:LN crystal by SFG pumped by the s-polarization 1878-nm strong laser beam. DFB: distributed feedback diode laser; TmDFA: Thulium-doped fiber amplifier; OI: optical isolator; AOM: acoustic optical modulator;  $\lambda/2$ : half-wave plate; PBS: polarization beam splitter cube; Att.: attenuator; s: s polarization; BCM: beam-combination mirror; HPFs: high-pass filters (852-nm high-transmission, 1560-nm and 1878-nm high-reflection mirrors); BPF: 852-nm band-pass filter (transmittances:  $\sim 75\%$ @852 nm,  $\sim 44\%$ @1560 nm and  $\sim 35\%$ @1878 nm, HMF bandwidth: 0.5 nm, OD4); SPCM: single-photon counting module.

of the PPMgO:LN crystal is found at a temperature of  $\sim 77.6^\circ\text{C}$ . The normalized results shown in Fig. 8.

For single-photon-level photon conversions it is known that noise, i.e., unwanted photons, at the target wavelength can be generated by the strong driving field. Many groups have also described the noise in the SFG experiments [17]. Fig. 9 shows the overview of SFG photonic conversion process from  $\lambda_2 = 1560.5$  nm to  $\lambda_1 = 852.3$  nm with the  $\lambda_p = 1878.0$  nm pump laser, the strong pump induced nonlinear processes (SPDC and SRS), and the cascaded conversion. First, pump laser will occur SPDC and SRS processes in nonlinear optical crystal. SPDC photons are located at the longer wavelength of the pump laser (marked by the cyan gridding part). SRS photons distribute on both sides of the pump light (marked by dark grey part). The SPDC, SRS and SHG photons, as well as the noise photons (generated by the cascaded SFG process and marked by the green part) located at the target output can be removed by using the HPFs and the narrow BPF.

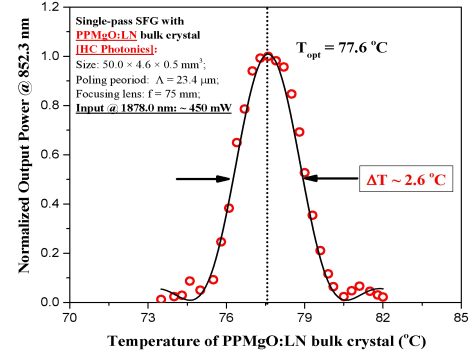


FIG. 8. Temperature dependence of 852.3-nm output power in the case of SFG. The open circles represent the experimental data, while the solid line is theoretical fitting curve. The optimal quasi-phase-matching temperature is  $77.6^\circ\text{C}$ , and the temperature bandwidth is  $\sim 2.6^\circ\text{C}$ .

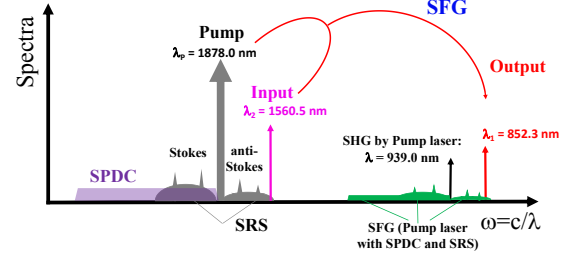


FIG. 9. Overview of SFG photonic conversion process from 1560.5 nm to 852.3 nm with the 1878.0-nm pump laser, the strong pump induced nonlinear processes, and the cascaded conversion. SPDC: the spontaneous parametric down-conversion (marked by the cyan gridding part); SRS: the spontaneous Raman scattering (Stokes and anti-Stokes photons, and marked by dark grey part); SHG: second-harmonic generation (939.0 nm and marked by the black arrow). The SPDC, SRS and SHG photons, as well as the noise photons (generated by the cascaded SFG process and marked by the green part) located at the target output can be removed by using the HPFs and the narrow BPF.

Different SNR and conversion efficiency can obtain by changing pump power. The definition of efficiency is the same as the DFG. These results shown in Fig. 10. The solid squares represent SNR, while the open circles represent the SFG conversion efficiency. The solid lines represents fit to Eq. (1). The SFG internal conversion efficiency is 2.0% with 150 mW pump laser, and the corresponding SNR is 4.6. If we use the filters with narrower bandwidth, the SNR will significantly improve. And we will also further improve the SNR by rotating polarization of output photons like DFG experiment. As the same as DFG results, the reason for efficiency saturation is mainly due to the imperfect matching of the waist spots and the mode volumes of pump laser and signal photons, and imperfect matching mainly causes the lower conver-

sion efficiency. In addition, the inverse DFG (from 852 nm to 1560 nm photons) is inevitable in the SFG experiment. This means that the 852 nm photons generated by the SFG may be further converted back to 1560 nm photons. Although the conversion efficiency of the inverse DFG is lesser than the target SFG, that factor may limits our SFG efficiency.

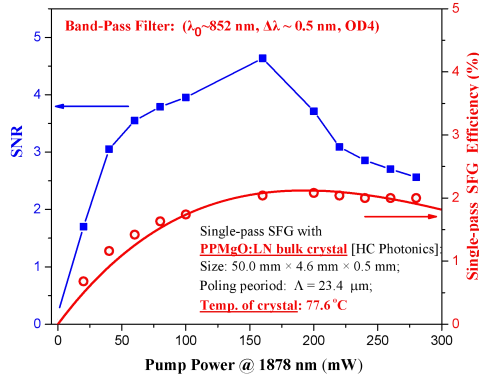


FIG. 10. Experimental data for SNR and SFG conversion efficiency versus 1878-nm pump power. The solid squares represent SNR, while the open circles represent SFG efficiency.

By adding second-harmonic generation (SHG) experiment (from 1560 nm to 780 nm laser) in this system, 852 nm and 780 nm lasers can be yielded simultaneously [30, 31]. Therefore, we can use this system in a cold atoms Rb-Cs two-component interferometer and in the formation of the RbCs dimer by the photoassociation of cold Rb and Cs atoms confined in a magneto-optical trap.

#### IV. CONCLUSIONS

We report the two-way single-photon-level photonic conversion between 852 nm and 1560 nm. First, the 852-

nm photons at cesium atomic D2 line have been converted (DFG) to 1560-nm photons at telecom C-band in a PPMgO:LN bulk crystal with strong pump field at 1878 nm. The DFG internal conversion efficiency is  $\sim 1.7\%$  with 150 mW pump laser mixing attenuated 852-nm laser pulses with a mean photon number per pulse is  $\sim 1$ , and the maximal SNR is 58.3. We can improve SNR by using narrower bandwidth filters and changing the polarization of the noises. Finally, SNR can promote nearly doubled than before. Then the 1560-nm photons at telecom C-band have been converted (SFG) to 852-nm photons at cesium atomic D2 line with the same conditions. The SFG internal conversion efficiency is  $\sim 2.0\%$  with 150 mW pump laser mixing attenuated 1560-nm laser pulses with a mean photon number per pulse is  $\sim 1$ , and the corresponding SNR is 4.6. In addition, we analyze the noise characteristics in conversion processes. In single-pass configuration, the optimum B-K focus factor  $\xi = 2.84$  is an important factor. The low conversion efficiency is mainly due to the mismatch of the waist spots and the mode volumes of pump laser and signal photons. In addition, if we use waveguide in this experiment, the efficiency will be greatly improved. This is benefit by the special structure of the waveguide.

The two-way conversion based on the same crystal can build a bridge between the quantum systems and realize the information transmission. This scheme can be extended to real single photons case, and combining our single photon source to realize the quantum network for ultra-low loss transmission in the future.

#### ACKNOWLEDGMENTS

This work is supported by the National Natural Science Foundation of China (NSFC 11774210, 61875111, 11974226 and 61905133), the National Key R&D Program of China (2017YFA0304502), Shanxi Provincial Graduate Innovation Project (PhD Candidates) (2019BY016) and the Shanxi Provincial 1331 Project for Key Subject Construction.

- 
- [1] H. J. Kimble, The quantum internet, *Nature*, **453**, 1023-1030 (2008).
  - [2] P. Kumar, Quantum frequency conversion, *Opt.Lett.*, **15**(24), 1476-1478 (1990).
  - [3] J. Huang and P. Kumar, Observation of quantum frequency conversion, *Phys.Rev.Lett.*, **68**(14), 2153-2156 (1992).
  - [4] D. Hucul, I. V. Inlek, G. Vittorini, C. Crocker, S. Debnath, S. M. Clark, and C. Monroe, Modular entanglement of atomic qubits using photons and phonons, *Nature Phys.*, **11**, 37-42 (2015).
  - [5] S. Ritter, C. Nolleke, C. Hahn, A. Reiserer, A. Neuzner, M. Uphoff, M. Mucke, E. Figueroa, J. Bochmann, and G. Rempe, An elementary quantum network of single atoms in optical cavities, *Nature*, **484**, 195-200 (2012).
  - [6] J. Hofmann, M. Krug, N. Ortegel, L. Gerard, M. Weber, W. Rosenfeld, and H. Weinfurter, Heralded entanglement between widely separated atoms, *Science*, **337**, 72-75 (2012).
  - [7] R. Stockill, M. J. Stanley, L. Huthmacher, E. Clarke, M. Hugues, A. J. Miller, C. Matthiesen, C. Le Gall, and M. Atatüre, Phase-tuned entangled state generation between distant spin qubits, *Phys.Rev.Lett.*, **119**(1), 010503 (2017).
  - [8] S. Zaske, A. Lenhard, C. A. Keler, J. Kettler, C. Hepp, C. Arend, R. Albrecht, W. M. Schulz, M. Jetter, P. Michler, and C. Becher, Visible-to-telecom quantum frequency conversion of light from a single quantum emitter, *Phys.Rev.Lett.*, **109**(14), 147404 (2012).
  - [9] S. Ates, I. Agha, A. Gulinatti, I. Rech, M. T. Rakher,

- A. Badolato, and K. Srinivasan, Two-photon interference using background-free quantum frequency conversion of single photons emitted by an InAs quantum dot, *Phys.Rev.Lett.*, **109**(14), 147405 (2012).
- [10] B. Albrecht, P. Farrera, X. Fernandez-Gonzalvo, M. Cristiani, and H. de Riedmatten, A waveguide frequency converter connecting rubidium-based quantum memories to the telecom C-band, *Nature Commun.*, **5**, 3376 (2014).
- [11] A. Dreau, A. Tcheborateva, A. E. Mahdaoui, C. Bonato, and R. Hanson, Quantum frequency conversion to telecom of single photons from a nitrogen-vacancy center in diamond, *Phys.Rev.Appl.*, **9**(6), 064031 (2018).
- [12] P. C. Strassmann, A. Martin, N. Gisin, and M. Afzelius, Spectral noise in frequency conversion from the visible to the telecommunication C-band, *Opt.Express*, **27**(10), 14298-14307 (2019).
- [13] H. Rutz, K. H. Luo, H. Suche, and C. Silberhorn, Quantum frequency conversion between infrared and ultraviolet, *Phys.Rev.Appl.*, **7**(2), 024021 (2017).
- [14] X. Fernandez-Gonzalvo, G. Corrielli, B. Albrecht, M. Grimaud, M. Cristiani, and H. de Riedmatten, Quantum frequency conversion of quantum memory compatible photons to telecommunication wavelengths, *Opt.Express*, **21**(17), 19473-19487 (2013).
- [15] S. Zaske, A. Lenhard, and C. Becker, Efficient frequency downconversion at the single photon level from the red spectral range to the telecommunications C-band, *Opt.Express*, **19**(13), 12825-12836 (2011).
- [16] J. S. Pelc, L. Ma, C. R. Phillips, Q. Zhang, C. Langrock, O. Slattery, X. Tang, and M. M. Fejer, Long-wavelength-pumped upconversion single-photon detector at 1550 nm: performance and noise analysis, *Opt.Express*, **19**(22), 21445-21456 (2011).
- [17] P. S. Kuo, J. S. Pelc, O. Slattery, Y. S. Kim, M. M. Fejer, and X. Tang, Reducing noise in single-photon-level frequency conversion, *Opt.Lett.*, **38**(8), 1310-1312 (2013).
- [18] K. Huang, X. R. Gu, M. Ren, Y. Jian, H. F. Pan, G. Wu, E. Wu, and H. P. Zeng, Photon-number-resolving detection at 1.04  $\mu\text{m}$  via coincidence frequency upconversion, *Opt.Lett.*, **36**(9), 1722-1724 (2011).
- [19] F. Ma, L. Y. Liang, J. P. Chen, Y. Gao, M. Y. Zheng, X. P. Xie, H. Liu, Q. Zhang, and J. W. Pan, Upconversion single-photon detectors based on integrated periodically poled lithium niobate waveguides, *J.Opt.Soc.Am.B*, **35**(9), 2096-2101 (2018).
- [20] T. Wright, R. Francis-Jones, C. Gawith, J. Becker, P. Ledingham, P. Smith, J. Nunn, P. Mosley, B. Brecht, and I. Walmsley, Two-way photonic interface for linking the  $\text{Sr}^+$  transition at 422 nm to the telecommunication C band, *Phys.Rev.Appl.*, **10**(4), 044012 (2018).
- [21] B. Liu, G. Jin, J. He, and J. M. Wang, Suppression of single-cesium-atom heating in a microscopic optical dipole trap for demonstration of an 852-nm triggered single-photon source, *Phys.Rev.A*, **94**(1), 013409 (2016).
- [22] G. Jin, B. Liu, J. He, and J. M. Wang, High on/off ratio nanosecond laser pulses for a triggered single-photon source, *Appl.Phys.Express*, **9**(7), 072702 (2016).
- [23] B. Liu, G. Jin, J. He, R. Sun, and J. M. Wang, Measurement of magic-wavelength optical dipole trap by using the laser-induced fluorescence spectra of trapped single cesium atoms, *Opt.Express*, **25**(14), 15861-15867 (2017).
- [24] K. S. Chaitanya, G. K. Samanta, and M. Ebrahim-Zadeh, High-power, single-frequency, continuous-wave second-harmonic-generation of ytterbium fiber laser in PPKTP and MgO:sPPLT, *Opt.Express*, **17**(16), 13711-13726 (2009).
- [25] G. D. Boyd and D. A. Kleinman, Parametric interaction of focused Gaussian light beams, *J.Appl.Phys.*, **39**(8), 3597-3639 (1968).
- [26] X. R. Gu, K. Huang, H. F. Pan, E. Wu, and H. P. Zeng, Photon correlation in single-photon frequency upconversion, *Opt.Express*, **20**(3), 2399-2407 (2012).
- [27] S. Vasilyev, A. Nevsky, I. Ernsting, M. Hansen, J. Shen, and S. Schiller, Compact all-solid-state continuous-wave single-frequency UV source with frequency stabilization for laser cooling of  $\text{Be}^+$  ions, *Appl.Phys.B*, **103**, 27-33 (2011).
- [28] A. Muller, O. B. Jensen, K. H. Hasler, B. Sumpf, G. Erbert, P. E. Andersen, and P. M. Petersen, Efficient concept for generation of diffraction-limited green light by sum-frequency generation of spectrally combined tapered diode lasers *Opt.Lett.*, **37**(18), 3753-3755 (2012).
- [29] M. Tawfieg, O. B. Jensen, A. K. Hansen, B. Sumpf, K. Paschke, and P. E. Andersen, Efficient generation of 509 nm light by sum-frequency mixing between two tapered diode lasers, *Opt.Comm.*, **339**, 137-140 (2015).
- [30] K. Zhang, J. He, and J. M. Wang, Single-pass laser frequency conversion to 780.2 nm and 852.3 nm based on PPMgO:LN bulk crystals and diode-laser-seeded fiber amplifiers, *Appl.Sci.*, **9**(22), 4942 (2019).
- [31] D. Clement, Z. Nassim, B. Yannick, C. Malo, and B. Alexandre, Multi-line fiber laser system for cesium and rubidium atom interferometry, *Opt.Express*, **25** (15), 16898-16906 (2017).